

MIT Open Access Articles

*Impact of deposition conditions on the
crystallization kinetics of amorphous GeTe films*

The MIT Faculty has made this article openly available. **Please share**
how this access benefits you. Your story matters.

Citation: Khoo, Chee Ying, Hai Liu, Wardhana A. Sasangka, Riko I. Made, Nobu Tamura, Martin Kunz, Arief S. Budiman, Chee Lip Gan, and Carl V. Thompson. "Impact of Deposition Conditions on the Crystallization Kinetics of Amorphous GeTe Films." *Journal of Materials Science* 51, no. 4 (October 20, 2015): 1864–1872.

As Published: <http://dx.doi.org/10.1007/s10853-015-9493-z>

Publisher: Springer US

Persistent URL: <http://hdl.handle.net/1721.1/103352>

Version: Author's final manuscript: final author's manuscript post peer review, without publisher's formatting or copy editing

Terms of use: Creative Commons Attribution-Noncommercial-Share Alike



1 ***Impact of deposition conditions on the crystallization kinetics of amorphous***
2 ***GeTe films***
3

4 Chee Ying Khoo^{1,2} • Hai Liu¹ • Wardhana.A. Sasangka³ • Riko I Made³ • Nobu Tamura⁴ • Martin Kunz⁴
5 • Arief S. Budiman⁵ • Chee Lip Gan^{1,2,3,*} • Carl V. Thompson^{2,3,6,#}
6

7 **Abstract** The speed at which phase change memory devices can operate depends strongly on the crystallization
8 kinetics of the amorphous phase. To better understand factors that affect the crystallization rate, we have
9 investigated crystallization of GeTe films as a function of their deposition temperatures and deposition rates,
10 using X-ray synchrotron radiation and Raman spectroscopy. As-deposited films were found to be fully
11 amorphous under all conditions, even though films deposited at higher temperatures and lower rates
12 experienced lower effective quench rates. Non-isothermal transformation curves show that the apparent
13 crystallization temperature of GeTe films decreases with increasing deposition temperature and decreasing
14 deposition rate. It was found that this correlates with a decrease in the activation energy for nucleation
15 (calculated using Kissinger’s analysis), while the activation energy for crystal growth remained unaffected.
16 From Raman spectroscopy measurements, it was found that increasing the deposition temperature or decreasing
17 the deposition rate, and therefore the effective quench rate, reduces the number of homopolar Te-Te bonds and
18 thereby reduces the barrier to crystal nucleation.

19 *Chee Lip Gan
20 clgan@ntu.edu.sg
21

22 #Carl V. Thompson
23 cthomp@mit.edu
24

25 ¹ School of Materials, Science and Engineering, Nanyang Technological University, Singapore 639798
26

27 ² Advance Materials for Micro- and Nano-Systems, Singapore-MIT Alliance, Singapore 117576
28

29 ³ Low Energy Electronic Systems, Singapore-MIT Alliance for Research and Technology, Singapore
30 138602
31

32 ⁴ Advance Light Source, Lawrence Berkeley National Lab, Berkeley, California 94720, USA
33

34 ⁵ Engineering Products Development (EPD) Pillars, Singapore University of Technology and Design,
35 Singapore 138682
36

37 ⁶ Department of Materials Science and Engineering, Massachusetts Institute of Technology, Cambridge,
38 Massachusetts 02139, USA
39
40

44 **Introduction**

45 In the mid-1960s, S.R. Ovshinsky proposed the idea of phase change recording [1]. Phase change materials (e.g.
46 $\text{Ge}_2\text{Sb}_2\text{Te}_5$ and GeTe) undergo a reversible transformation between crystalline and amorphous states when
47 subjected to laser-induced or current-induced heating and quenching [2,3]. The attractiveness of phase change
48 materials lies in their very large changes in electrical resistivity and optical reflectivity when switching between
49 these two states [4-6]. This phenomenon is currently used in optical information storage and is under wide-
50 spread investigation for use in electrical information storage devices [7,8]. The operation of these devices
51 strongly depends on the crystallization temperatures and crystallization rates of the materials, and therefore a
52 detailed understanding of factors that influence the kinetics of crystallization is critical. Studies of amorphous
53 $\text{Ge}_2\text{Sb}_2\text{Te}_5$ and GeTe films prepared using different methods, such as sputtering, melt-quenching and ion-
54 irradiation have been carried out [9,10]. The local order of these amorphous films has been examined using
55 Raman spectroscopy and was found to be significantly different [9,10]. These differences were found to
56 correlate with differences in crystallization temperatures [9,10].

57 In this work, we report studies of the crystallization kinetics of amorphous GeTe as a function of deposition
58 temperature and deposition rate. The crystallization temperature is determined using x-ray synchrotron radiation
59 during in-situ annealing. Effective activation energies for the crystallization process were determined using
60 Kissinger's analysis [11]. The local order of the as-deposited amorphous GeTe films was analyzed using micro-
61 Raman spectroscopy.

62

63 **Experimental Procedures**

64 1 μm -thick GeTe films were deposited by RF-magnetron sputtering from stoichiometric targets onto Si
65 substrates coated with thin layers of native SiO_2 . The background pressure before sputtering was maintained at
66 $\sim 10^{-6}$ Torr. With the presence of argon gas during sputtering, the pressure was maintained at 10^{-3} Torr. A first
67 set of samples was deposited on substrates at room temperature, 60 °C, 80 °C and 100 °C, with a deposition rate
68 of 8 nm/min. For a second set of samples, films were deposited at room temperature using different rates, 7.1
69 nm/min, 8.8 nm/min and 10.3 nm/min, by varying the argon gas pressure. For both sets of experiments, real-
70 time synchrotron x-ray diffraction with a 2D detector and monochromatic beam (energy = 10 keV, $\lambda = 0.124$
71 nm) at beamline 12.3.2 of the Advanced Light Source in the Lawrence Berkeley National Laboratory was used
72 to monitor the crystallization. Each exposure time was set to be 60 seconds. The synchrotron X-ray beam has a
73 final focus size of 2 μm (v) x 8 μm (h) (FWHM). The diffraction patterns were collected with a DECTRIS

74 Pilatus 1 M pixel area detector (active area of 179 mm x 169 mm), which was placed at a distance of
75 approximately 140 mm from the sample. More detailed information on the set up at this beamline can be
76 obtained elsewhere [12,13].

77 All samples were annealed at a constant rate of 2 °C/min, 5 °C/min or 10 °C/min from room temperature to
78 230 °C, a temperature at which they were fully crystalline. Transformation curves at different heating rates were
79 obtained by determining the fraction of the film that had transformed as a function of temperature. The
80 microstructures of the GeTe films were characterized using energy dispersive x-ray spectroscopy (EDX) and
81 transmission electron microscopy (TEM). A focused ion beam (FIB) system with dual-beam capability was used
82 to prepare the TEM samples and a JEOL TEM 2100F with an accelerating voltage of 200 kV was used to
83 examine the as-deposited films. EDX was used to determine the composition of the films used in this
84 experiment.

85 All the as-deposited amorphous GeTe thin films were also analyzed by means of micro-Raman
86 spectroscopy. The samples were excited with a He-Ne laser ($\lambda = 633$ nm) and the incident laser power was
87 adjusted to 0.5 mW in order to minimize heating effects in the illuminated sample region of interest [9,14]. The
88 Raman spectra were recorded at an interval of 0.4 cm^{-1} . Accumulation times of 3 minutes were sufficient to
89 obtain a satisfactory signal-to-noise ratio.

90

91 **Results and discussion**

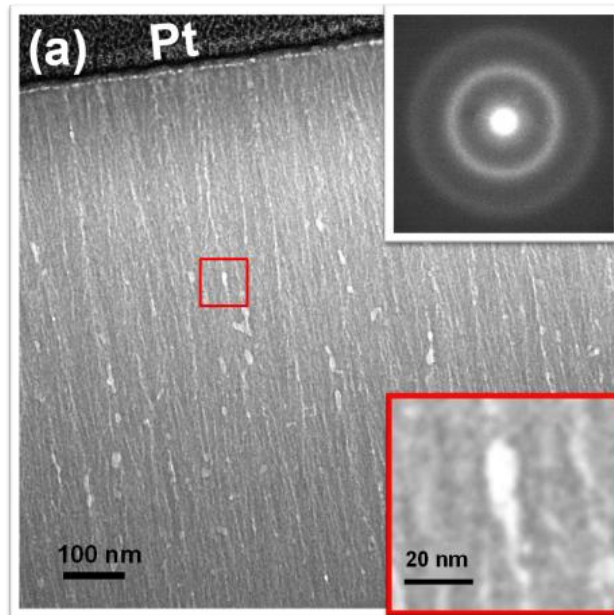
92

93 *Effect of deposition temperatures*

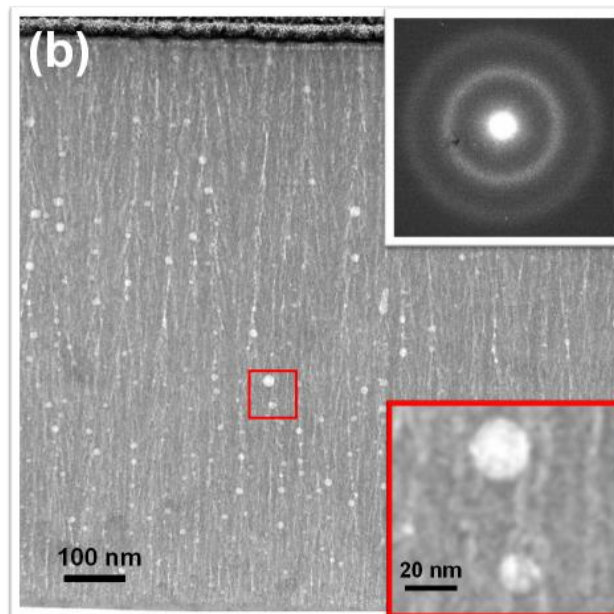
94

95 Figure 1 shows bright field TEM images of GeTe films deposited at room temperature and 100 °C. Cross-
96 sectional TEM images reveal that all as-deposited films were fully amorphous, but with columnar structures and
97 nano-scale voids. The latter is not uncommon in amorphous films deposited using sputter deposition [15,16].
98 The inset electron diffraction patterns confirm that the films were amorphous as deposited, which was also
99 supported by x-ray diffraction (XRD) analysis. From EDX, the composition of the films was determined to be
100 $\text{Ge}_{43}\text{Te}_{57}$ ($\pm 1\%$ error), which is Te-rich.

101



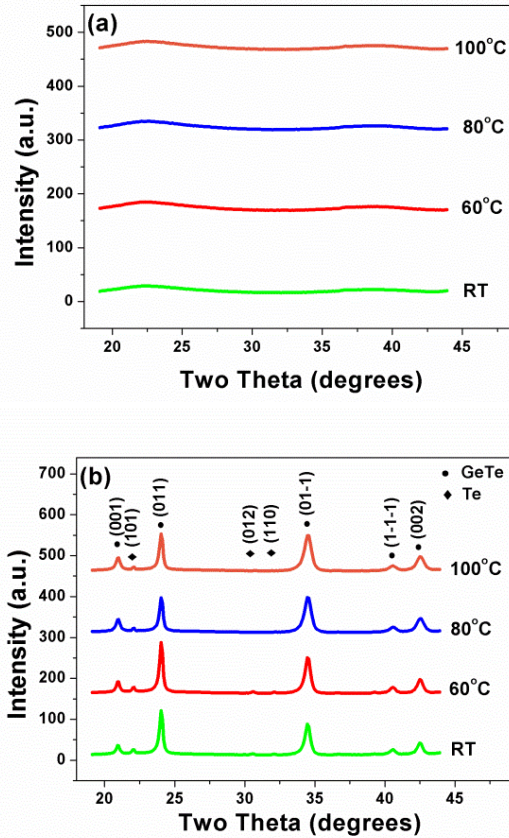
102



103 **Fig. 1** Bright field TEM images of cross-sections of GeTe films deposited at (a) room temperature and (b) 100
104 °C on Si substrates coated with thin layers of native oxide. Top right insets show electron diffraction patterns
105 and bottom right insets show high magnification views of nano-scale voids within the film. Pt layers on top of
106 the films act as protective layers during FIB sample preparation.

107 Debye-Scherrer rings were generated based on diffraction intensities from the 2D detector integrated in the
108 azimuthal direction. Figure 2 shows XRD results obtained by transforming 2D synchrotron data using XMAS, a
109 software developed in-house at beamline 12.3.2 [17]. The as-deposited films were amorphous at all deposition
110 temperatures, as shown in figure 2a. After annealing to 230 °C, the films were found to be fully crystallized, as
111 shown in figure 2b. Regardless of the deposition temperatures, the GeTe films were composed of the same

112 phase, with the expected trigonal symmetry [18]. Weak Te peaks were also observed due to the Te-rich
113 composition of the films.



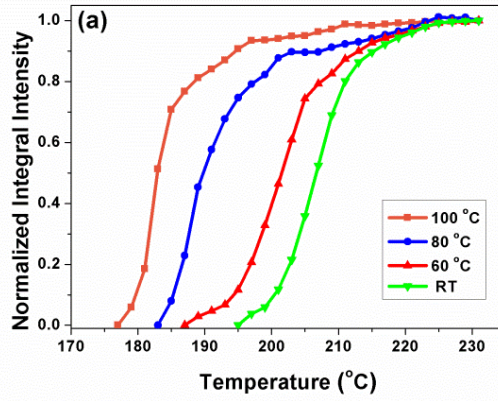
114

115

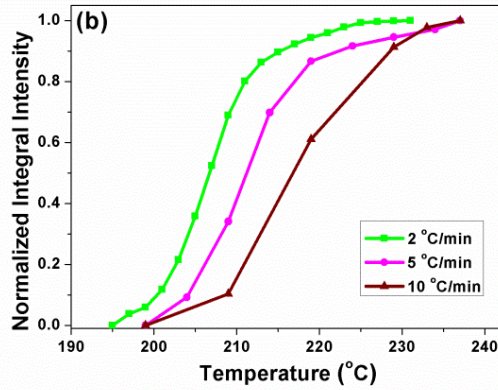
116 **Fig. 2** XRD results for GeTe films (a) as-deposited and (b) fully crystallized at 230 °C, for films deposited at
117 different substrate temperatures (room temperature, 60 °C, 80 °C and 100 °C).

118 Figure 3a shows transformation curves for crystallization of GeTe, based on the maximum intensity of the
119 (011) peak normalized by the maximum intensity of this peak after full transformation at 230 °C. The sample
120 was heated at a rate of 2 °C/min from room temperature to 230 °C. The apparent crystallization temperature was
121 defined as the temperature at which half of the sample was crystallized [19]. The apparent crystallization
122 temperatures observed in this study are higher than values reported by others, as determined from optical
123 reflectivity measurements [20,21]. This is expected as all the films here are Te-rich in composition. From the
124 transformation curves, it is clearly seen that the apparent crystallization temperatures decrease with increasing
125 deposition temperature. Figure 3b shows transformation curves for GeTe films deposited at room temperature
126 and heated at different rates: 2 °C/min, 5 °C/min and 10 °C/min. As expected, the apparent crystallization
127 temperature increases with increasing heating rate [22,23].

128



129



130 **Fig. 3 (a)** Transformation curves for GeTe films deposited at different temperatures, based on normalized
 131 magnitudes of the (011) peak observed at 230 °C. The heating rate was 2 °C/min. **(b)** Transformation curves for
 132 GeTe films deposited at room temperature and heated at different rates.

133 Figure 4a shows the local effective activation energy E_c as a function of the fraction transformed α . E_c was
 134 determined using the Kissinger method for various values of α for data obtained at different heating rates shown
 135 in Figure 3b [11]. The Kissinger equation can be written as follows,

$$136 \ln\left(\frac{\beta}{T_c^2}\right) = -\frac{E_c}{kT_c} + const, \quad (1)$$

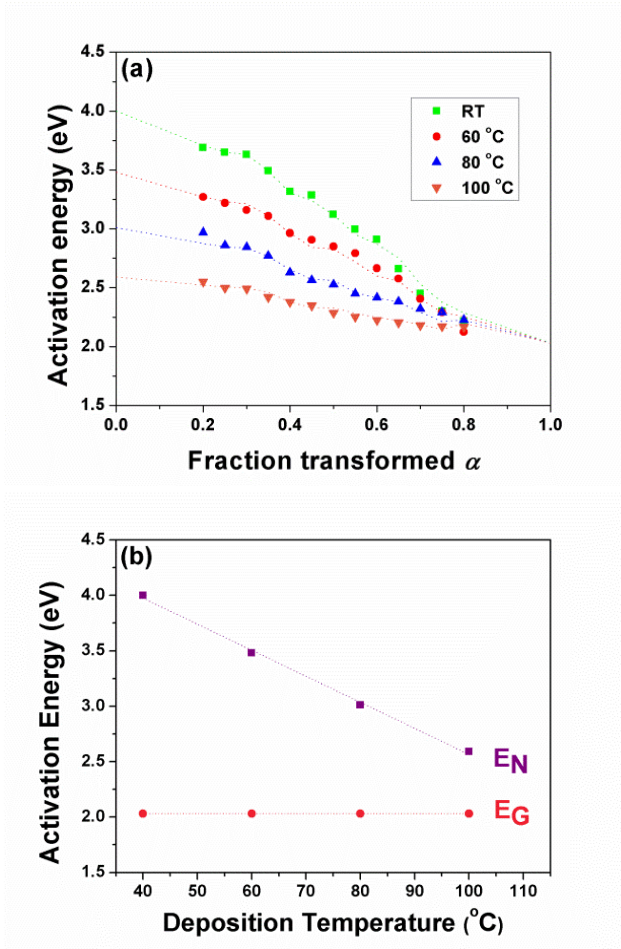
137 where β is the heating rate, k is Boltzmann's constant, E_c is the activation energy at a particular transformed
 138 fraction α and T_c is the temperature at which the transformed fraction α is reached.

139 The dependence of E_c on the fraction transformed is affected by changes in the nucleation and growth
 140 behavior during the crystallization process [24-26]. The local activation energy $E_c(\alpha)$ is composed of two parts,
 141 the activation energy of nucleation (E_n) and the activation energy of growth (E_g) [27-29]. E_c at a given α can be
 142 written as,

$$143 E_\alpha = aE_n + bE_g \quad (I \geq 0, U \geq 0), \quad (2)$$

144 where I and U are the steady state nucleation rate and growth velocity respectively, with a and b are two
145 variables related to the Avrami parameter, having values $0 \leq a, b \leq 1$ and $a + b = 1$ [28,29]. In the early stage of
146 transformation, with lower values of α , crystallization is dominated by nucleation whereas at later stages, higher
147 values of α , crystallization is dominated by growth. Fitting the plot in Figure 4a using a non-linear regression
148 method (shown using dotted lines), we estimated the value of the activation energies for nucleation and growth,
149 $E_c(\alpha=0) = E_n$ and growth $E_c(\alpha=1) = E_g$, respectively. The fitting was carried out under the assumption that the
150 values of a and b at a particular value of α are the same for all deposition temperatures. Figure 4b shows values
151 of the activation energies for nucleation and growth obtained from Figure 4a. It is seen that the activation energy
152 for nucleation decreases significantly with increasing deposition temperature, from 4.0 eV to 2.6 eV. In contrast,
153 the activation energy for growth remains relatively constant at 2.0 eV. Thus, the decrease in the effective
154 activation energy for crystallization of GeTe observed for increasing deposition temperatures is primarily due to
155 a reduction in the activation energy for nucleation. Similar activation energies for nucleation and growth of
156 films deposited at room temperature have been reported elsewhere using a different technique [10,30]. Films
157 deposited at room temperature experience a higher effective quench rate as compared to films deposited at
158 higher temperatures [31]. We postulate that this results in fewer clusters that can act as precursors of crystalline
159 nuclei, thus making nucleation more difficult. That the activation energy for growth is unaffected by the
160 deposition conditions may explain why it has been found in other studies that samples having the same
161 composition but made under different conditions have the same temperature dependence for crystallization,
162 while differences in the crystallization rate are still observed due to differences in the nucleation rates [32,33].

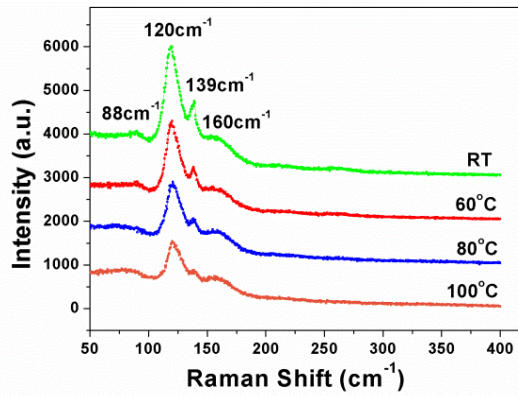
163



164

165 **Fig. 4 (a)** The local effective activation energy E_α as a function of the fraction transformed α for films prepared
166 at various deposition temperatures and **(b)** activation energies for nucleation and growth as a function of the
167 deposition temperature.

168 Figure 5 shows Raman spectra for GeTe films deposited at different temperatures. For all the Raman
169 spectra, there are peaks found at 88 cm^{-1} , 120 cm^{-1} , 139 cm^{-1} and 160 cm^{-1} . The broad peaks found at 88 cm^{-1}
170 and 160 cm^{-1} are contributed by Ge-Te vibration modes [14,34,35]. Two distinct peaks were also observed at
171 120 cm^{-1} and 139 cm^{-1} , and their intensity decreased with increasing deposition temperature. It is known that
172 crystalline Tellurium has strongest peaks at $120.4 \pm 0.5 \text{ cm}^{-1}$ and $140.7 \pm 0.5 \text{ cm}^{-1}$ [36]. The close proximity of
173 the observed peaks suggests the presence of homopolar Te-Te bonds in the as-deposited state. It is known that
174 homopolar Te-Te bonds are forbidden in the crystalline structure [10]. It has therefore been suggested that the
175 presence of these homopolar Te-Te bonds might retard the crystallization process [9]. Our results suggest that
176 the specific effect of Te-Te homopolar bonds is to raise the barrier for nucleation of the crystalline phase, rather
177 than to impede crystal growth.



178

179 **Fig. 5** Raman spectra for amorphous GeTe films prepared at various deposition temperatures.

180

181 *Effect of deposition rates*

182

183 Figure 6 shows bright field TEM images of GeTe films deposited at deposition rates of 7.1 nm/min and 10.3

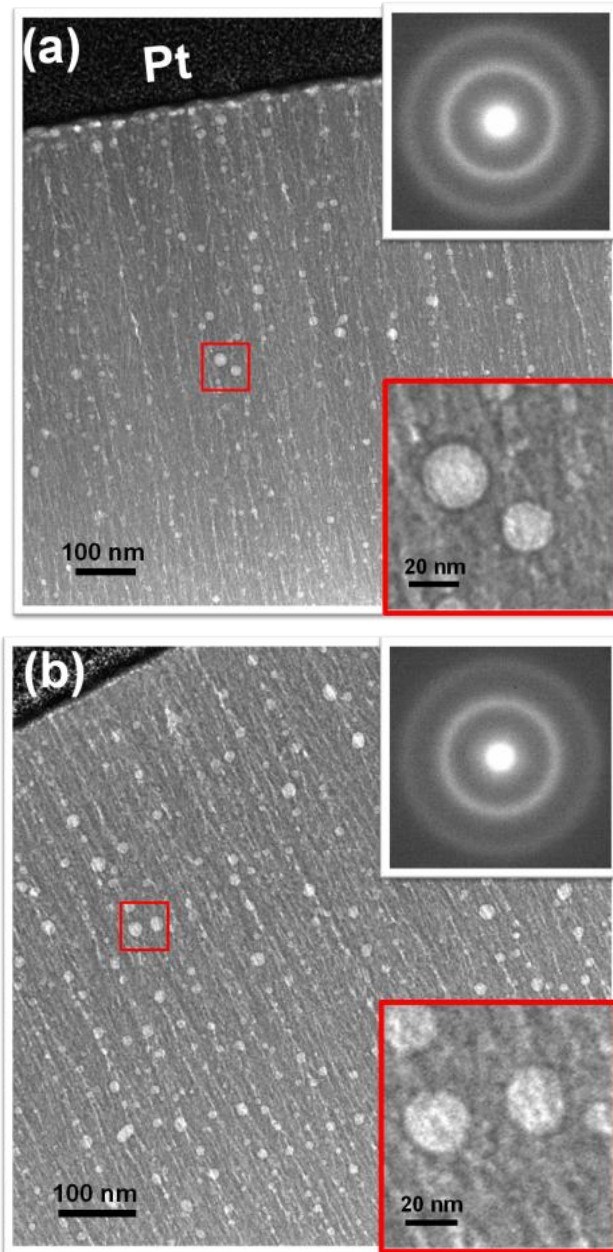
184 nm/min. The observed structures are similar to those of the films deposited at different temperatures (Fig. 1).

185 The inset electron diffraction patterns confirm that the films are amorphous as deposited, which was also

186 supported by XRD analysis. Using EDX, the composition of the films was determined to be $\text{Ge}_{47}\text{Te}_{53}$ ($\pm 1\%$),

187 independent of the Ar pressure and sputtering rate.

188

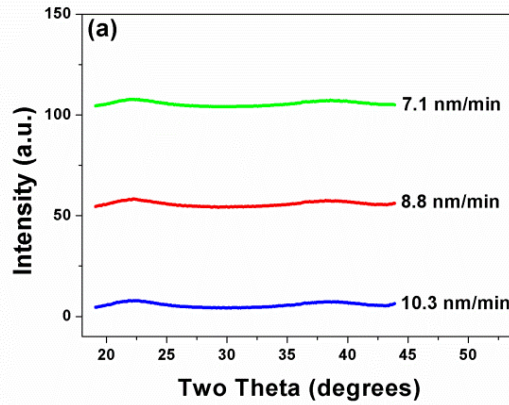


189

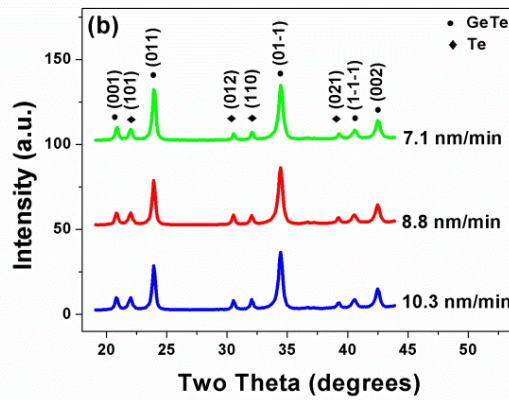
190 **Fig. 6** Bright field TEM images of cross sections of GeTe films deposited at deposition rates of (a) 7.1 nm/min
191 and (b) 10.3 nm/min, on Si substrates coated with thin layers of native oxide. Top right insets show electron
192 diffraction patterns and bottom right insets show high magnification views of nano-scale voids within the film.
193 Pt layers on top of the films act as protective layers during FIB sample preparation.

194 Figure 7 shows XRD results for these films deposited at different sputtering rates. The as-deposited films
195 were amorphous at all deposition rates, as shown in figure 7a. After annealing to 235 °C, the films were found to
196 be fully crystallized, as shown in figure 7b. Regardless of the deposition rate, weak Te peaks were also observed
197 due to the Te-rich composition of the films.

198



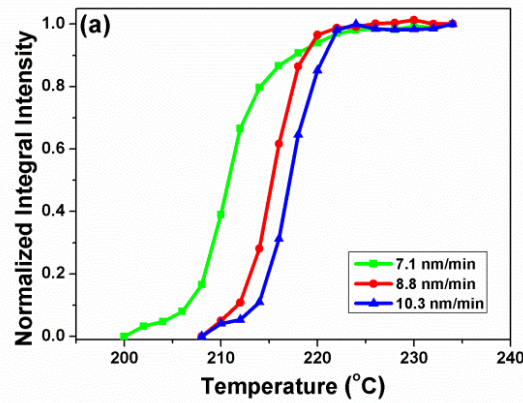
199



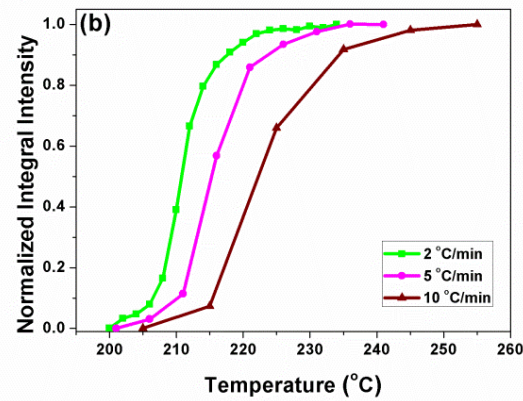
200 **Fig. 7** XRD results for GeTe films (a) as-deposited and (b) fully crystallized at 235 °C, for films deposited at
201 different deposition rates.

202 Figure 8a shows transformation curves for crystallization of GeTe, based on the maximum intensity of the
203 (011) peak normalized by the magnitude of this peak after full transformation at 235 °C. . The samples were
204 heated at a rate of 2 °C/min from room temperature to 235 °C. From the transformation curves, it is clearly seen
205 that the apparent crystallization temperatures increase with increasing deposition rate. Figure 8b shows
206 transformation curves for GeTe films deposited at a deposition rate of 7.1 nm/min and heated at different rates:
207 2 °C/min, 5 °C/min and 10 °C/min.

208



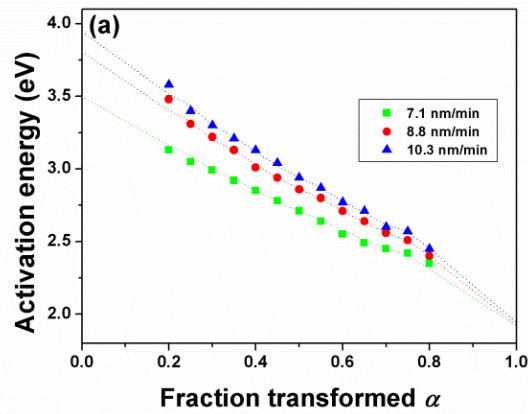
209



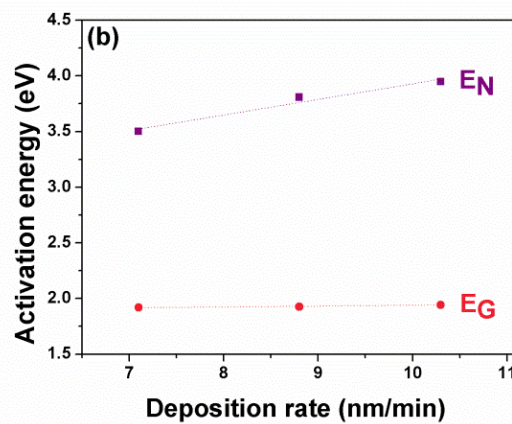
210 **Fig. 8 (a)** Transformation curves for GeTe films deposited at different deposition rates, normalized by the
211 magnitude of the (011) peak observed at 235 °C, with a heating rate of 2 °C/min and **(b)** transformation curves
212 for GeTe films deposited at deposition rate of 7.1 nm/min and heated at different rates.

213 The same approach discussed earlier was used to obtain the local effective activation energy E_a as a
214 function of the fraction transformed α as shown in Figure 9a. Figure 9b shows values of the activation energies
215 for nucleation and growth obtained from the data in Figure 9a. It is seen that the activation energy for nucleation
216 increases with increasing deposition rate, from 3.5 eV to 4.0 eV. In contrast, the activation energy for growth
217 remains constant at a value of 1.9 eV. Thus, the increase in the effective activation energy for crystallization of
218 GeTe observed for increasing deposition rates is primarily due to an increase in the activation energy for
219 nucleation. It is expected that films deposited at higher deposition rates experience a higher effective quench
220 rate [31]. This dependence on the effective quench rate is consistent with the results obtained for films deposited
221 as different temperatures.

222

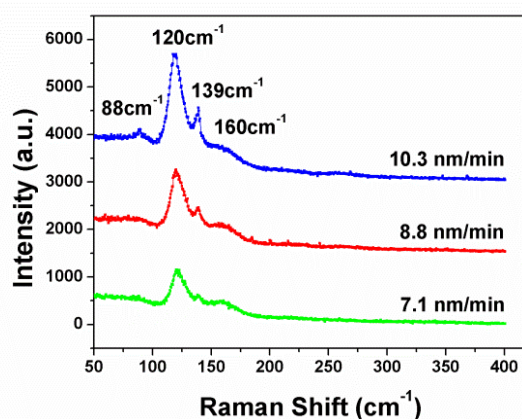


223



224 **Fig. 9 (a)** The local effective activation energy E_{α} as a function of fraction transformed α for films prepared at
225 various deposition rates and **(b)** activation energies for nucleation and growth as a function of the deposition
226 rate.

227 Figure 10 shows Raman spectra for GeTe films deposited at different deposition rates. Similar to what was
228 found for films deposited at different temperature, two distinct peaks were also observed at 120 cm^{-1} and 139
229 cm^{-1} , and their intensity increased with increasing deposition rate. This suggests the presence of homopolar Te-
230 Te bonds in all the as-deposited films regardless of the sputtering rate. However, this also shows that the number
231 of Te-Te homopolar bonds increases with increasing deposition rate, which, we suggest, raises the barrier for
232 nucleation of the crystalline phase.



233

234 **Fig. 10** Raman spectra for amorphous GeTe films prepared at various deposition rates.

235 Different sputtering targets were used in both set of experiments. It should be noted that the film deposited
 236 at room temperature in the first set of experiments exhibits higher activation energies for nucleation as
 237 compared to those in the second set of experiments. This is likely due to the higher amount of excess Te in the
 238 first set of film, resulting from the use of different sputtering targets for the two sets of films. Work done by
 239 Carria *et al.* has shown that increasing amounts of excess Te will lead to a higher activation energy for
 240 crystallization [21]. However, this does not affect our interpretation of the data within a single set of samples
 241 having a fixed amount of excess Te, and the correspondence of the trends observed for both sets. It has been
 242 shown through experiments carried out by others that Te-Te homopolar bonds exist even in stoichiometric
 243 amorphous GeTe films [37,38]. We have also carried out experiments on stoichiometric Ge₂Sb₂Te₅ films
 244 deposited at varying substrate temperatures, with the XRD results and Raman spectra shown in Figures S1 and
 245 S2 (Online Resource 1). Even with stoichiometric Ge₂Sb₂Te₅ samples, the intensity of the 120 cm⁻¹ Raman peak
 246 changes with the substrate temperature in a way that is analogous to what is seen for GeTe, and there are
 247 corresponding analogous changes in the crystallization behavior. This is consistent with other reported
 248 observations on stoichiometric GeTe and Ge₂Sb₂Te₅ films in which the crystallization rate is observed to
 249 decrease with the increased presence of homopolar Te-Te bonds [9,10]. Taken together, these results support
 250 our proposition that the Te-Te bond density is the critical factor that affects crystal nucleation in the as-
 251 deposited films.

252

253 **Summary and Conclusions**

254 We have studied the crystallization of amorphous GeTe films prepared by sputter deposition onto substrates
 255 held at different temperatures and deposited at different sputtering rates. Through analysis of the crystallization

256 process carried out at different heating rates, it is shown that the deposition temperature and deposition rate have
257 a significant effect on the nucleation of the crystalline phase, but a negligible effect on its growth. The activation
258 energy for crystal nucleation increased with decreasing deposition temperature and with increasing deposition
259 rate. Decreasing the deposition temperature and increasing the deposition rate both increase the effective
260 quench rate. This highlights the influence of the effective quench rate on the crystallization of phase change
261 materials. Raman spectral analysis indicates an increase of the number of homopolar Te-Te bonds with
262 decreasing deposition temperature or increasing deposition rate. Given that homopolar bonds do not exist in the
263 crystalline phase, we suggest that it is clustering of Te atoms in the films deposited at low temperatures and high
264 rates that raises the barrier to nucleation of the crystalline phase.

265

266 **Acknowledgements** The X-ray synchrotron experiments were carried out at Beamline 12.3.2 of the Advanced
267 Light Source at Lawrence Berkeley National Laboratory, which is supported by the Director, Office of Science,
268 Office of Basic Energy Sciences, Materials Sciences Division, of the U.S. Department of Energy under Contract
269 No. DE-AC02-05CH11231 at Lawrence Berkeley National Laboratory and University of California, Berkeley,
270 California. The move of the micro-diffraction program from ALS beamline 7.3.3 onto to the ALS superbend
271 source 12.3.2 was enabled through the NSF grant #0416243. Special thanks to Mr. Xinglin Wen for assistance
272 in carrying out Raman spectroscopy and Mr. Yu Gao for his help in using the Lingo software. The authors
273 would also like to thank the Singapore-MIT Alliance for funding this work and for providing a scholarship for
274 C.Y. Khoo. The electron microscopy work was carried out in the Facility for Analysis, Characterization, Testing
275 and Simulation (FACTS) in Nanyang Technological University, Singapore.

276

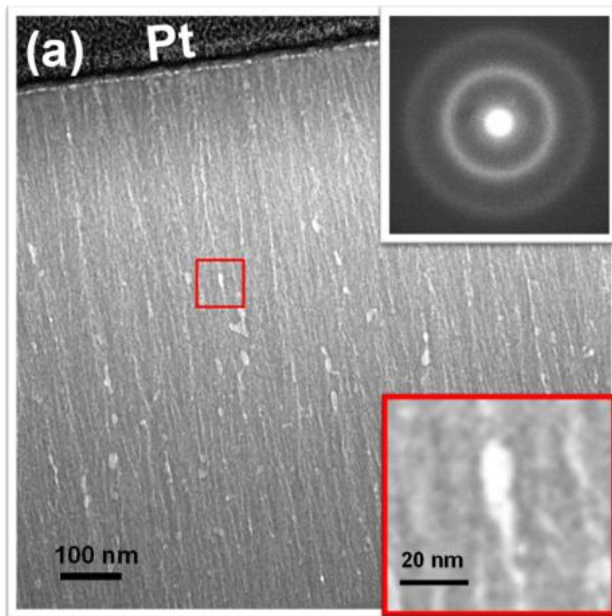
277 **References**

278

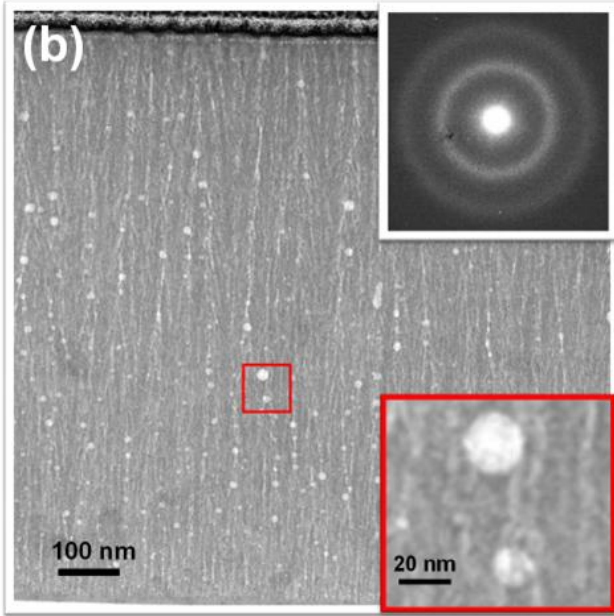
- 279 1. Ovshinsky SR (1968) Reversible electrical switching phenomena in disordered structures. *Physical Review*
280 *Letters* 21 (20):1450-1453
- 281 2. Kolobov AV, Fons P, Tominaga J (2007) Phase-change optical recording: past, present, future. *Thin Solid*
282 *Films* 515 (19):7534-7537
- 283 3. Wetnic W, Wuttig M (2008) Reversible switching in phase-change materials. *Materials Today* 11 (6):20-27.
284 doi:10.1016/S1369-7021(08)70118-4
- 285 4. Kolobov AV, Fons P, Frenkel AI, Ankudinov AL, Tominaga J, Uruga T (2004) Understanding the phase-
286 change mechanism of rewritable optical media. *Nature Materials* 3 (Copyright 2005, IEE):703-708
- 287 5. Wuttig M, Yamada N (2007) Phase-change materials for rewriteable data storage. *Nature Materials* 6
288 (Compendex):824-832
- 289 6. Lencer D, Salinga M, Grabowski B, Hickel T, Neugebauer J, Wuttig M (2008) A map for phase-change
290 materials. *Nature Materials* 7 (Copyright 2009, The Institution of Engineering and Technology):972-977
- 291 7. Raoux S, Wenig W, Lelmini D (2010) Phase change materials and their application to nonvolatile memories.
292 *Chemical Reviews* 110 (1):240-267. doi:10.1021/cr900040x
- 293 8. Lencer D, Salinga M, Wuttig M (2011) Design rules for phase-change materials in data storage applications.
294 *Advanced Materials* 23 (18):2030-2058. doi:10.1002/adma.201004255

- 295 9. Carria E, Mio AM, Gibilisco S, Miritello M, d'Acapito F, Grimaldi MG, Rimini E (2011) Polymorphism of
296 Amorphous $\text{Ge}_2\text{Sb}_2\text{Te}_5$ Probed by EXAFS and Raman Spectroscopy. *Electrochemical and Solid-State Letters* 14
297 (12):480-482. doi:10.1149/2.019112esl
- 298 10. Mio AM, Carria E, D'Arrigo G, Gibilisco S, Miritello M, Grimaldi MG, Rimini E (2011) Nucleation and
299 grain growth in as deposited and ion implanted GeTe thin films. *Journal of Non-Crystalline Solids* 357
300 (10):2197-2201. doi:http://dx.doi.org/10.1016/j.jnoncrysol.2011.02.042
- 301 11. Kissinger HE (1957) Reaction Kinetics in Differential Thermal Analysis. *Analytical Chemistry* 29
302 (11):1702-1706
- 303 12. Tamura N, MacDowell AA, Spolenak R, Valek BC, Bravman JC, Brown WL, Celestre RS, Padmore HA,
304 Batterman BW, Patel JR (2003) Scanning X-ray microdiffraction with submicrometer white beam for
305 strain/stress and orientation mapping in thin films. *Journal of Synchrotron Radiation* 10:137-143.
306 doi:10.1107/S0909049502021362
- 307 13. Kunz M, Tamura N, Chen K, MacDowell AA, Celestre RS, Church MM, Fakra S, Domning EE, Glossinger
308 JM, Kirschman JL, Morrison GY, Plate DW, Smith BV, Warwick T, Yashchuk VV, Padmore HA, Ustundag E
309 (2009) A dedicated superbend x-ray microdiffraction beamline for materials, geo-, and environmental sciences
310 at the advanced light source. *The Review of scientific instruments* 80 (3):035108. doi:10.1063/1.3096295
- 311 14. Andrikopoulos KS, Yannopoulos SN, Voyiatzis GA, Kolobov AV, Ribes M, Tominaga J (2006) Raman
312 scattering study of the a-GeTe structure and possible mechanism for the amorphous to crystal transition. *Journal*
313 *of Physics: Condensed Matter* 18 (3):965-979. doi:10.1088/0953-8984/18/3/014
- 314 15. Bales GS, Zangwill A (1991) Macroscopic model for columnar growth of amorphous films by sputter
315 deposition. *Journal of Vacuum Science & Technology A (Vacuum, Surfaces, and Films)* 9 (1):145-149.
316 doi:10.1116/1.577116
- 317 16. Tsukimoto S, Moriyama M, Murakami M (2004) Microstructure of amorphous tantalum nitride thin films.
318 *Thin Solid Films* 460 (1-2):222-226. doi:10.1016/j.tsf.2004.01.073
- 319 17. Tamura N (2014) XMAS: a versatile tool for analyzing synchrotron x-ray microdiffraction data, in *Strain*
320 *and Dislocation Gradients from Diffraction: Spatially-Resolved Local Structure and Defects*. Imperial College
321 Press, London, United Kingdom
- 322 18. Matsunaga T, Kojima R, Yamada N, Kifune K, Kubota Y, Tabata Y, Takata M (2006) Single Structure
323 Widely Distributed in a GeTe– Sb_2Te_3 Pseudobinary System: A Rock Salt Structure is Retained by Intrinsically
324 Containing an Enormous Number of Vacancies within its Crystal. *Inorganic Chemistry* 45 (5):2235-2241.
325 doi:10.1021/ic051677w
- 326 19. Ghezzi GE, Morel R, Brenac A, Boudet N, Audier M, Fillot F, Maitrejean S, Hippert F (2012)
327 Crystallization of $\text{Ge}_2\text{Sb}_2\text{Te}_5$ nanometric phase change material clusters made by gas-phase condensation.
328 *Applied Physics Letters* 101 (23):233113-233114
- 329 20. Gourvest E, Lhostis S, Kreisel J, Armand M, Maitrejean S, Roule A, Vallee C (2009) Evidence of
330 Germanium precipitation in phase-change $\text{Ge}_{1-x}\text{Te}_x$ thin films by Raman scattering. *Applied Physics Letters* 95
331 (3):031908 (031903 pp.). doi:10.1063/1.3186077
- 332 21. Carria E, Mio AM, Gibilisco S, Miritello M, Bongiorno C, Grimaldi MG, Rimini E (2012) Amorphous-
333 crystal phase transitions in $\text{Ge}_x\text{Te}_{1-x}$ alloys. *Journal of the Electrochemical Society* 159 (2):H130-H139.
334 doi:10.1149/2.048202jes
- 335 22. Friedrich I, Weidenhof V, Njoroge W, Franz P, Wuttig M (2000) Structural transformations of $\text{Ge}_2\text{Sb}_2\text{Te}_5$
336 films studied by electrical resistance measurements. *Journal of Applied Physics* 87 (9):4130-4134
- 337 23. Choi Y, Jung M, Lee Y-K (2009) Effect of heating rate on the activation energy for crystallization of
338 amorphous $\text{Ge}_2\text{Sb}_2\text{Te}_5$ thin film. *Electrochemical and Solid-State Letters* 12 (7):F17-F19.
339 doi:10.1149/1.3129137
- 340 24. Abu El-Oyoun M (2009) Determination of the crystallization kinetic parameters of $\text{Ge}_{22.5}\text{Te}_{77.5}$ glass using
341 model-free and model-fitting methods. *Journal of Alloys and Compounds* 486 (1-2):1-8.
342 doi:10.1016/j.jallcom.2009.06.137
- 343 25. Kasyap S, Patel A, Pratap A (2014) Crystallization kinetics of $\text{Ti}_{20}\text{Zr}_{20}\text{Cu}_{60}$ metallic glass by isoconversional
344 methods using modulated differential scanning calorimetry. *J Therm Anal Calorim* 116 (3):1325-1336.
345 doi:10.1007/s10973-014-3753-z
- 346 26. Dohare C, Mehta N (2012) Iso-conversional kinetic study of non-isothermal crystallization in glassy
347 $\text{Se}_{98}\text{Ag}_2$ alloy. *J Therm Anal Calorim* 109 (1):247-253. doi:10.1007/s10973-011-1696-1
- 348 27. Wei L, Biao Y, Wen-hai H (2005) Complex primary crystallization kinetics of amorphous Finemet alloy.
349 *Journal of Non-Crystalline Solids* 351 (40-42):3320-3324. doi:10.1016/j.jnoncrysol.2005.08.018
- 350 28. Majhi K, Varma KBR (2009) Crystallization kinetic studies of $\text{CaBi}_2\text{B}_2\text{O}_7$ glasses by non-isothermal
351 methods. *Journal of Materials Science* 44 (2):385-391. doi:10.1007/s10853-008-3149-1
- 352 29. Soares RS, Monteiro RCC, Lima MMRA, Sava BA, Elisa M (2014) Phase transformation and
353 microstructural evolution after heat treatment of a terbium-doped lithium-aluminum phosphate glass. *Journal of*
354 *Materials Science* 49 (13):4601-4611. doi:10.1007/s10853-014-8162-y

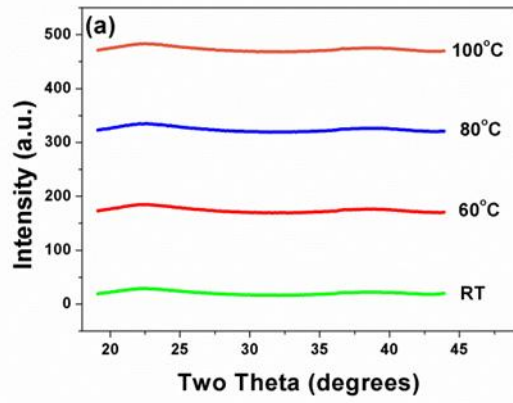
- 355 30. Lu QM, Libera M (1995) Microstructural measurements of amorphous GeTe crystallization by hot-stage
356 optical microscopy. *Journal of Applied Physics* 77 (2):517-521. doi:http://dx.doi.org/10.1063/1.359034
357 31. Chu JP, Lai YW, Lin TN, Wang SF (2000) Deposition and characterization of TiNi-base thin films by
358 sputtering. *Materials Science & Engineering A (Structural Materials: Properties, Microstructure and Processing)*
359 A277 (1-2):11-17. doi:10.1016/S0921-5093(99)00560-2
360 32. Jeyasingh R, Fong SW, Lee J, Li Z, Chang K-W, Mantegazza D, Asheghi M, Goodson KE, Wong HSP
361 (2014) Ultrafast characterization of phase-change material crystallization properties in the melt-quenched
362 amorphous phase. *Nano Letters* 14 (6):3419-3426. doi:10.1021/nl500940z
363 33. Orava J, Hewak DW, Greer AL (2015) Fragile-to-Strong Crossover in Supercooled Liquid Ag-In-Sb-Te
364 Studied by Ultrafast Calorimetry. *Advanced Functional Materials* 25 (30):4851-4858.
365 doi:10.1002/adfm.201501607
366 34. Andrikopoulos KS, Yannopoulos SN, Kolobov AV, Fons P, Tominaga J (2007) Raman scattering study of
367 GeTe and Ge₂Sb₂Te₅ phase-change materials. *Journal of Physics and Chemistry of Solids* 68 (5-6):1074-1078.
368 doi:10.1016/j.jpcs.2007.02.027
369 35. Mazzarello R, Caravati S, Angioletti-Uberti S, Bernasconi M, Parrinello M (2010) Signature of Tetrahedral
370 Ge in the Raman Spectrum of Amorphous Phase-Change Materials. *Physical Review Letters* 104 (8):085503
371 36. Pine AS, Dresselhaus G (1971) Raman Spectra and Lattice Dynamics of Tellurium. *Physical Review B* 4
372 (2):356-371
373 37. G. Fisher, J. Tauc, Verhelle Y (1974) *Amorphous and Liquid Semiconductors*. vol 2. London
374 38. Hosokawa S, Hari Y, Kouchi T, Ono I, Sato H, Taniguchi M, Hiraya A, Takata Y, Kosugi N, Watanabe M
375 (1998) Electronic structures and local atomic configurations in amorphous GeSe and GeTe. *Journal of Physics:*
376 *Condensed Matter* 10 (8):1931-1950. doi:10.1088/0953-8984/10/8/024
377



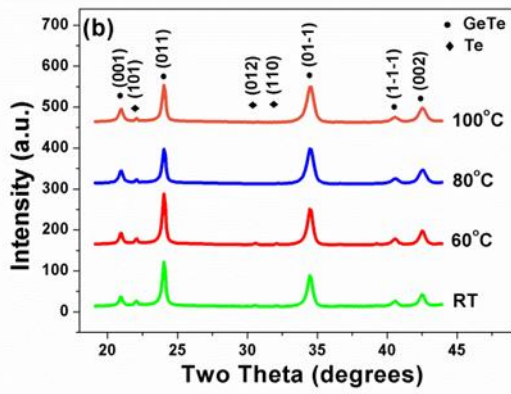
378



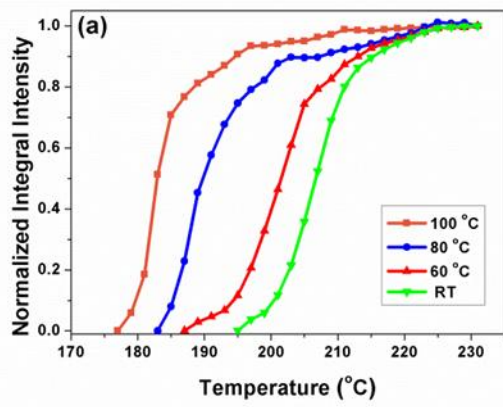
379



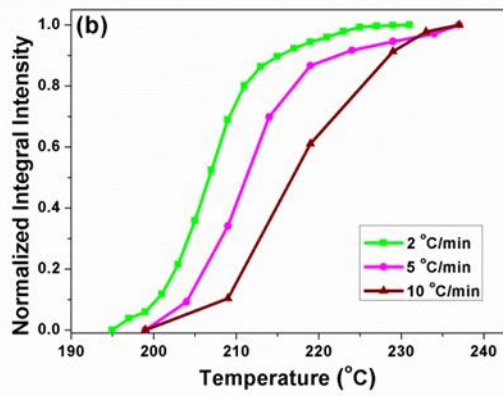
380



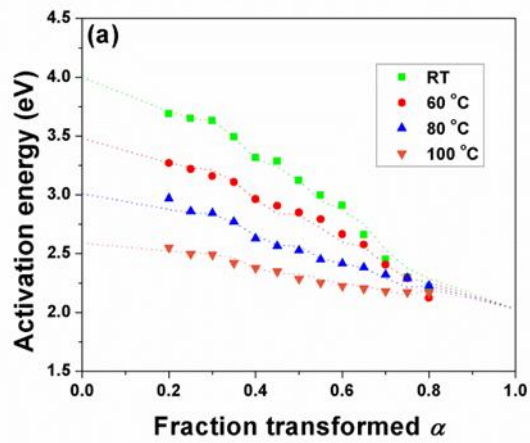
381



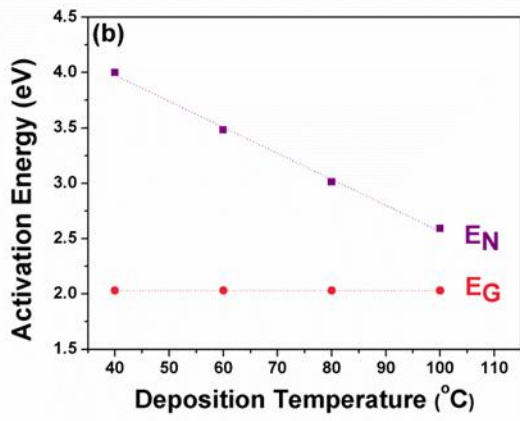
382



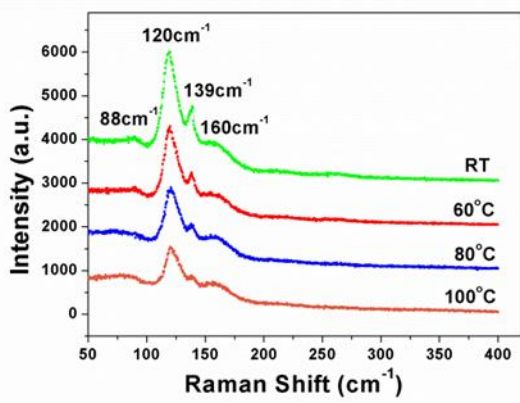
383



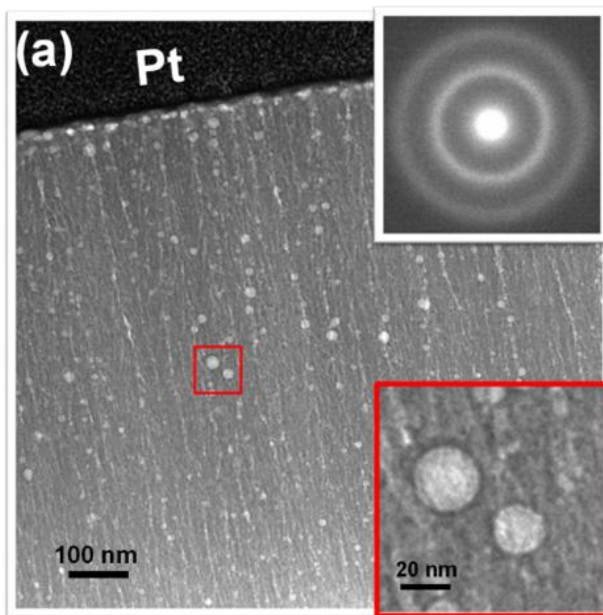
384



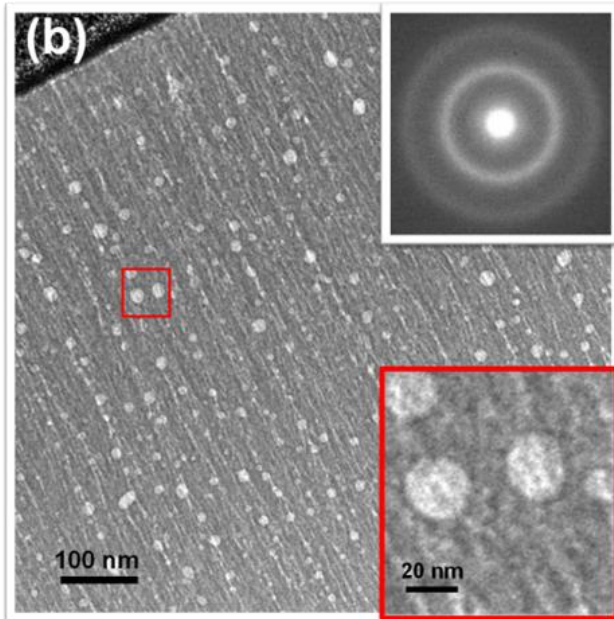
385



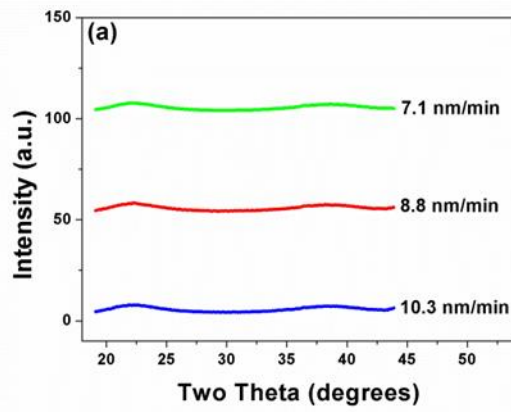
386



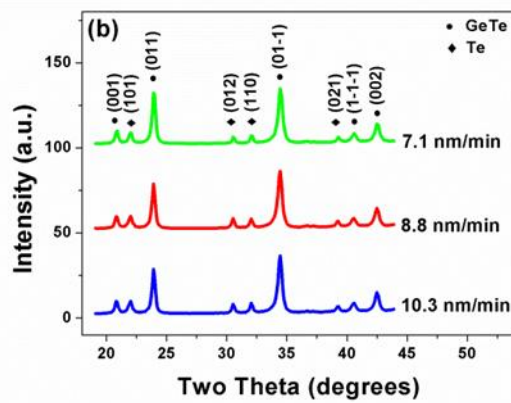
387



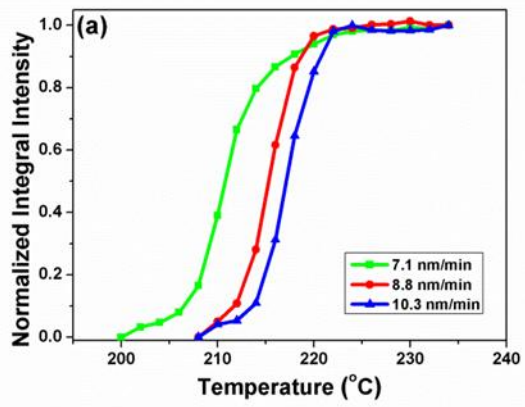
388



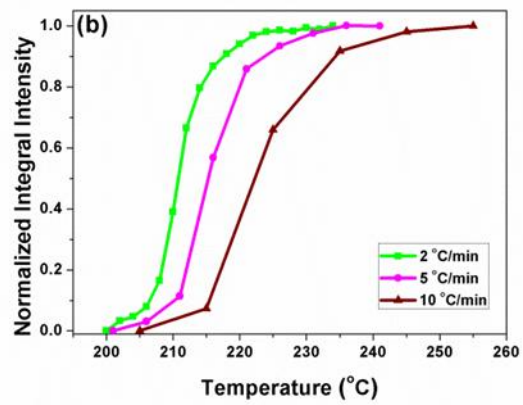
389



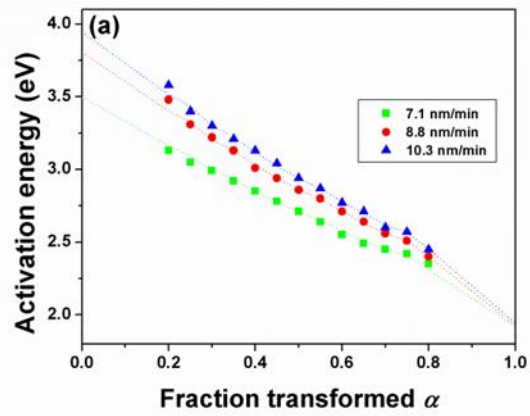
390



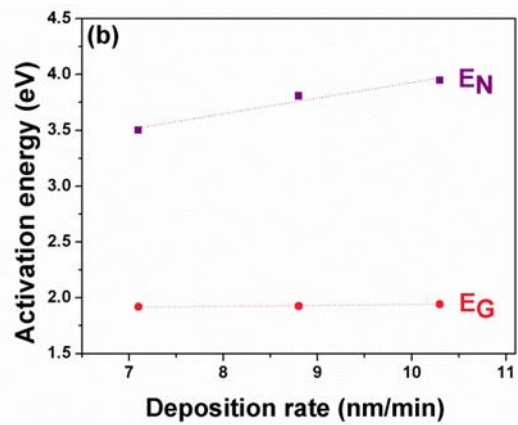
391



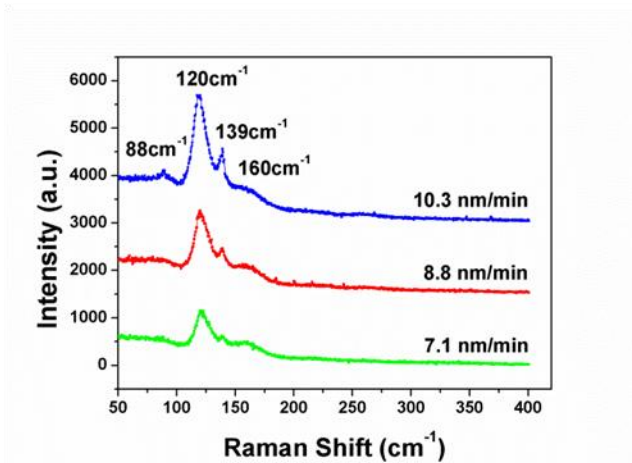
392



393



394



395